

A Comparison Between MHD Modeling and Experimental Results in a 3-Phase AC Arc Plasma Torch: Influence of the Electrode Tip Geometry

Christophe Rehmet · Frédéric Fabry · Vandad Rohani ·
François Cauneau · Laurent Fulcheri

Received: 11 December 2013 / Accepted: 19 February 2014 / Published online: 4 March 2014
© Springer Science+Business Media New York 2014

Abstract Arc behavior in 3-Phase AC plasma technology remains poorly explored. This system noticeably differs from the classical DC plasma torches and aims to overcome certain limitations, such as efficiency, equipment cost and reliability. A MHD model of a 3-Phase AC plasma torch was recently developed at Mines-ParisTech. The model does not include the electrodes in the computational domain. In parallel, experiments were conducted using a high-speed video camera shooting 100,000 frames per second. In this paper, the comparison between MHD modeling and experimental results shows that the arc behavior is in line with the results from the MHD model. Particularly, the strong influences of both the electrode jets and Lorentz forces on the arc motion are confirmed. However, some differences between experimental and numerical electrical waveforms are observed and particularly in the current–voltage phase shift. A new model was then developed by integrating the electrodes into the computational domain and adjusting the electrode tip geometry. With this simulation, we were able to reproduce the phase shift, power and voltage values with a good accuracy showing the strong influence of electrode tip geometry on the 3-Phase arc plasma discharge.

Keywords 3-Phase AC plasma torch · MHD modeling · Electric arc behavior · Electrode tip geometry

Introduction

A lot of studies have been dedicated to DC thermal plasma torches [1, 2], but very few have been conducted on non-transferred AC plasma torches. Indeed, most of the industrial

C. Rehmet (✉) · F. Fabry · V. Rohani · F. Cauneau · L. Fulcheri
Centre Procédés, Energies Renouvelables et Systèmes Energétiques (PERSEE), MINES ParisTech,
CS 10207, rue Claude Daunesse, 06904 Sophia Antipolis Cedex, France
e-mail: christophe.rehmet@mines-paristech.fr

L. Fulcheri
e-mail: laurent.fulcheri@mines-paristech.fr

applications are based on DC plasma torches with water cooled electrodes [3–5]. A 3-Phase AC plasma technology with high temperature consumable graphite electrodes has been under development at MINES-ParisTech for about 20 years. This technology noticeably differs from the classical DC plasma torches and aims to overcome a number of limits of DC torches, for some specific applications such as gasification or plasma-assisted combustion. These limitations are mainly related to the relatively high equipment and operating costs in DC technologies which are due to: (1) the limited electrode lifetime [6] and (2) the sensitive electronics included in the current rectifier. 3-Phase AC power supplies have proven their durability and reliability for many years in the steel industry at power reaching up to 500 MW. According to Fabry et al. [4], for future industrial scale development of the Waste-to-Energy gasification processes based on thermal plasma, it appears that 3-Phase plasma torches using cheap consumable parts such as graphite electrodes could be a solution to reliability and equipment/operating cost issues making this plasma technology less complex and more reliable.

AC plasma torches have been explored in Japan [7], Russia (for AC plasma generators with rail electrodes [8, 9] or rod electrodes [10, 11]) and France. Ravary et al. [12] and Weidong et al. [13] have studied 3-Phase arc behavior with a medium-speed camera (7,000 fps). They studied a geometry composed of three converging graphite electrodes located on three lines located over a 15° revolution cone (120° between each line). The authors demonstrated that, in such geometry, the interaction of phase currents on each other induces strong rotating magnetic repulsive forces leading to a global centrifugal motion of the arcs. With the improvement of video camera technologies, it is now possible to record high-speed phenomena such as those encountered in arcs up to 100,000 frames per second [14–16]. Recently, the analysis of a 3-Phase AC plasma torch has been carried out using a 100,000 fps high-speed video camera and an oscilloscope for the arc motion and electrical signal analyses respectively. Detailed experimental results have been presented in Ref. [17].

While very few MHD models have been developed for AC plasma systems [18–20], a MHD model of the 3-Phase plasma torch has recently been successfully developed [21] using Code_Saturne[®] software [22]. The MHD model automatically simulates arc ignition, extinction and motion between the three electrode tips. Significant information that can hardly be achieved experimentally has been obtained with this modeling. To improve the simulation, the model has been modified by adjusting the electrode tips geometry and integrating the electrodes into the computational domain. The results of this model are discussed in this paper.

First the MHD model is presented. Then the main characteristics of the experimental setup are described. Later the comparison between the previous model and experimental results based on current and inter-electrode gap variation is discussed. Next the experimental and MHD current and voltage waveforms are compared. To improve the simulation, the model has been modified by integrating the electrode into the computational domain. The results are presented in this section. To conclude, the influence of the electrode tip geometry on the plasma flow and discharge stability is highlighted.

3-Phase AC Plasma Experimental Setup

The 3-Phase plasma experimental set up is composed of three radial graphite electrodes whose axes are located in a plane perpendicular to the reactor axis, as represented in Fig. 1. The diameter of the electrodes is 17 mm. These arcs are entrained in a gas flow and initiated at the tip of the electrodes connected to a 3-Phase AC power supply [12].

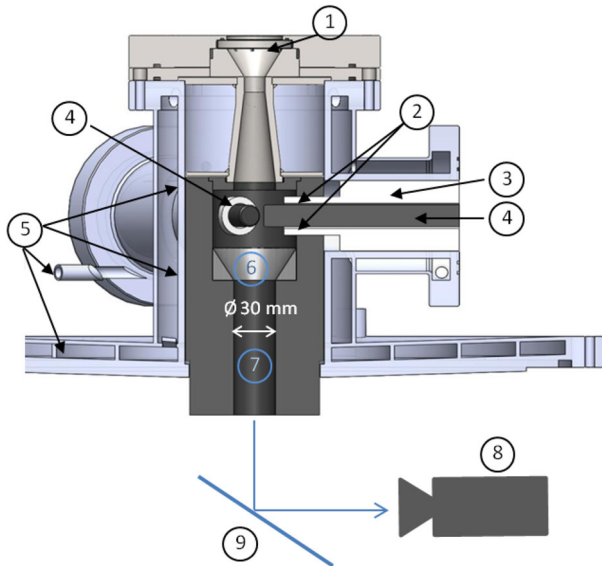


Fig. 1 Geometry of the 3-Phase AC plasma system with the three radial electrodes in the same plan and perpendicular to the reactor axis. **1** Entrance of the central plasma gas injection; **2** Annular sheathing gas inlet around the electrodes; **3** Electrical insulation; **4** 17 mm diameter graphite electrodes; **5** Water cooling; **6** Arc zone; **7** 30 mm diameter plasma flow outlet; **8** High-speed video camera; **9** Mirror

Depending on the characteristics of the power supply, the frequency can vary between grid one (50–60 Hz) up to higher frequencies (several kHz). In this study, a 263 kW 3-Phase converter (rectifier-chopper-inverter) was used and the frequency was set at 666–680 Hz.

Video camera analysis was carried out using a high-speed Olympus FS [23] video camera with a 100,000 fps shooting rate, 10 μ s exposure time and 112×80 pixels, giving a 0.425 mm width per pixel on the raw images recorded with the camera. Equipped with an F-mount lens, the camera is located at an optical distance of about 2 m from the electrode tips. Various optical filters were used to adjust the image brightness. Contrast, luminosity, and image treatment were also adjusted afterwards with an adequate imaging post-treatment.

Voltage measurements were carried out with a differential ST 1,000 probe. As represented in Fig. 2, a 1:100 ratio current transducer was implemented on each phase to allow for current measurements. The current signal was obtained by measuring the voltage on a load resistance of $10 \Omega \pm 5 \%$. Current and voltage measurements were performed with a two channel oscilloscope (Agilent DSO1004A) on Phase 3. As summarized in Table 1, experiments were realized by varying RMS phase current, nitrogen plasma gas flow rate, and inter-electrode gap.

MHD Modeling of the 3-Phase AC Plasma Torch

Assumptions

The study was carried out for an arc discharge operating with nitrogen. Property data are taken from [24]. The 3-D model of the 3-Phase system is based on the following commonly used main assumptions.

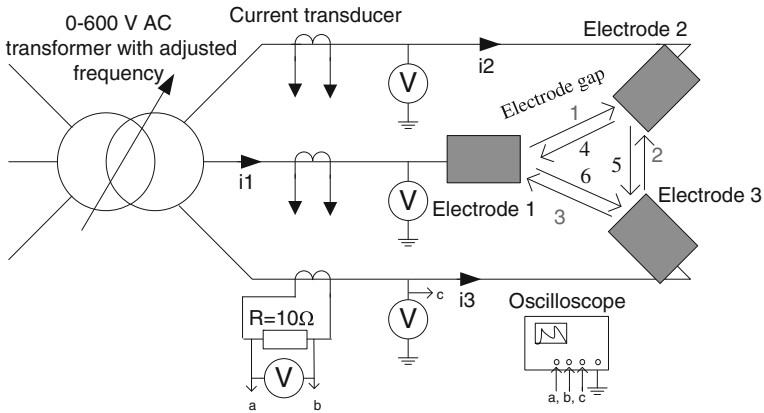


Fig. 2 Simplified representation of the 3-Phase AC plasma circuit with electrical measurements. Arrows numbered from 1 to 6 are a chronological representation of arc discharges for one period. *Arrows* indicate current direction

1. The gas is incompressible.
2. The gas flow is laminar and time dependent.
3. Inductive currents are neglected.
4. Gravitational effects and radiation are not taken into account.
5. Plasma is considered as a single continuous fluid (nitrogen) and at Local Thermodynamic Equilibrium (LTE).

The Reynolds number is less than 2,000, characteristic of a laminar gas flow regime. The Mach number was a posteriori confirmed always less than 0.3, characteristic of an incompressible gas.

The inductive currents are neglected as the power frequency supply (666 Hz) is much lower than the ion frequency or the radio frequency feeding ICP plasma torches (MHz).

The LTE assumption has been considered in this study to limit the calculation cost and because of the challenges of the 3-Phase system modeling. Obviously, this is a strong assumption and it would be interesting to develop a more sophisticated two-temperature non local thermodynamic equilibrium (nLTE) model in a later phase.

Radiation losses have been taken into account considering the net emission coefficient for air taken from Ref. [25]. The voltage drop in the near electrodes sheath is not considered for lack of basic knowledge of AC arcs. Therefore, the total voltage drop results in the voltage drop in the arc column.

Governing Equations

Considering the above-mentioned assumptions, the time dependent fluid conservation set of equations can be written as follows:

Mass conservation equation:

$$\frac{\partial \rho}{\partial t} + \text{div}(\rho \vec{V}) = 0 \tag{1}$$

where ρ and \vec{V} are the mass density and the velocity vector respectively.

Table 1 Summary of the operating parameters studied

	Current (A)	Inter-electrodes gap (mm)	Nitrogen plasma gas flow rate (Nm ³ h ⁻¹)
Case a	150–200	5.5	5
Case b	50–100	5.5	5
Case c	300	5.5	5
Case d	150–200	13	5
Case e	150–200	5.5	7

Momentum conservation equation:

$$\frac{\partial \rho \vec{V}}{\partial t} + \text{div}(\rho \vec{V} \otimes \vec{V}) = -\overrightarrow{\text{grad}}(p) + \text{div}(\overrightarrow{\tau}) + \vec{J} \wedge \vec{B} \tag{2}$$

where p , τ , \vec{J} , \vec{B} are the pressure, shear stress tensor, current density vector, and magnetic field vector, respectively. The term $\vec{J} \wedge \vec{B}$ represents the Laplace forces acting on the flow.

Energy conservation equation:

$$\frac{\partial \rho h}{\partial t} + \text{div}(\rho h \cdot \vec{V}) = +\text{div}\left(\frac{\lambda}{C_p} \overrightarrow{\text{grad}} h\right) + \vec{J} \cdot \vec{E} - S_{\text{rad}} \tag{3}$$

where h , λ , C_p , \vec{E} , $\vec{J} \cdot \vec{E}$ are the gas enthalpy, thermal conductivity, specific heat, electric field vector, and Joule effect, respectively.

Assuming simplified approximation of Ohm’s Law and electrical global neutrality, the set of Maxwell’s equations is defined by the following equations:

$$\vec{J} = \sigma \cdot \vec{E} \tag{4}$$

$$\vec{E} = -\overrightarrow{\text{grad}}(\phi) \tag{5}$$

$$\text{div}(\vec{J}) = \text{div}[\sigma \overrightarrow{\text{grad}}(\phi)] = 0 \tag{6}$$

$$\vec{B} = \text{rot} \cdot \vec{A} \tag{7}$$

$$\text{div}(\overrightarrow{\text{grad}} \vec{A}) = -\mu_0 \cdot \vec{J} \tag{8}$$

where σ , Φ , A and μ_0 are the electrical conductivity, electrical potential, vector potential, and vacuum permeability, respectively.

Geometry & Computational Grid

The grid mesh was created using the software Salome 6© [26]. The computational domain refers to the functional fluid area of the arc evolution (Fig. 3) as the simulation of the entire 3D reactor would be computationally too expensive. A non-uniform hexahedral mesh is used in all areas of the computational fluid domain. However, due to geometry-meshing issues, three limited external zones of the domain were excluded. Because they represent no more than 2 % of the total volume of the computational grid and are located far from the functional arc zone, we can assume that this meshing exclusion will not have a major influence on the overall calculation. The mesh contains 888,840 nodes. The domain is refined at the vicinity of the inter-electrode gap.

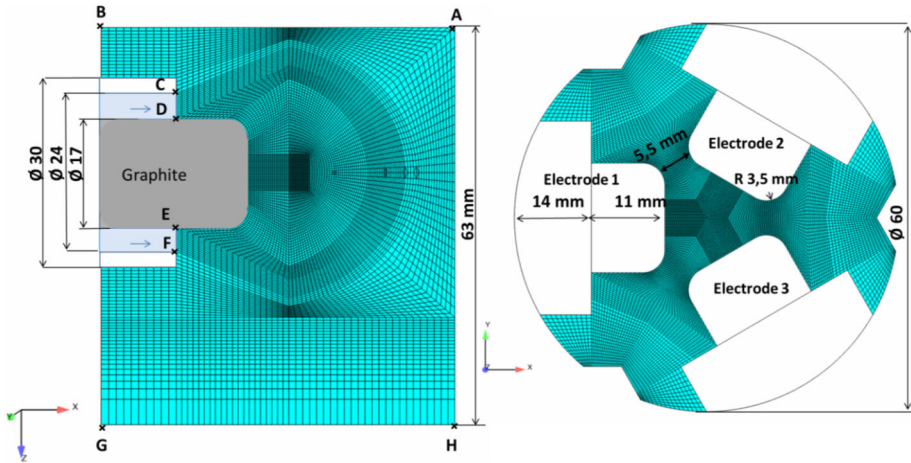


Fig. 3 Cross-sections of the 3-Phase plasma torch computational grid on the axis of one electrode (*left*) and on the three electrodes gap (*right*)

Table 2 Boundary conditions applied to a section of the computational domain, with f , t_{ref} and it the frequency, the times step and the iteration number, respectively

		Velocity (m.s ⁻¹)	Temperature	Φr (V)	P (Pa)	A
<i>AB</i>	Central injection	0.01–0.43	300 K	$\frac{\partial \phi r}{\partial n} = 0$	$\frac{\partial P}{\partial n} = 0$	$\frac{\partial A}{\partial n} = 0$
<i>BC, FG</i>	Walls	0	$\frac{\partial T}{\partial n} = 0$	$\frac{\partial \phi r}{\partial n} = 0$	$\frac{\partial P}{\partial n} = 0$	$\frac{\partial A}{\partial n} = 0$
<i>CD; EF</i>	Inlets around electrodes	1.0526	300 K	$\frac{\partial \phi r}{\partial n} = 0$	$\frac{\partial P}{\partial n} = 0$	$\frac{\partial A}{\partial n} = 0$
<i>DE</i>	Electrodes	0	$\frac{\partial T}{\partial n} = 0$	$\phi_r \sin(2\pi f t_{ref} it - \frac{2k\pi}{3}) *$	$\frac{\partial P}{\partial n} = 0$	$\frac{\partial A}{\partial n} = 0$
<i>GH</i>	Outflow	$\frac{\partial v}{\partial n} = 0$	$\frac{\partial T}{\partial n} = 0$	$\frac{\partial \phi r}{\partial n} = 0$	1.013×10^5	0

Boundary Conditions

The boundary conditions are detailed on Table 2 related to the cross-section view in Fig. 3. Regarding the hydrodynamic boundary conditions, the central plasma gas injection is located in the AB zone. For the first 2.5 ms (500 time steps), the velocity is 0.1 m s⁻¹ in order to allow for smooth arc ignition. Subsequently, for the following 2.5 m s⁻¹, a linear velocity ramp is applied at the inlet to increase the inflow from 0.1 to 0.43 m s⁻¹, giving a flow rate of 4.16 Nm³ h⁻¹. On CD and EF zones the annular sheathing inlet is located around the electrode. The imposed velocity is 1.05 m s⁻¹, giving a 1Nm³ h⁻¹ nitrogen flow rate on each inlet. Atmospheric pressure is imposed at the outlet.

Regarding the thermal conditions, a 300 K temperature in injected nitrogen is imposed. In this study, the walls are considered adiabatic. The modeling zone considered in this paper is very limited (6 cm height, 4 cm downstream the electrodes axis). In this modeling zone, the hot gas plasma flow remains very far from the walls due to cold gas sheathing at the vicinity of the walls resulting from the axial plasma gas injection. Therefore the adiabatic condition can reasonably be considered. A 4,300 K temperature is imposed at the

electrodes tip. This value is the average temperature obtained on the tip of the graphite electrodes using a bi-chromatic pyrometer mounted on the experimental set up.

Regarding the electromagnetic conditions, a 666 Hz sinusoidal electrical potential waveform is imposed on each electrode. This electrical potential is $2\pi/3$ phase shifted between the three electrodes and is iteratively adjusted by the model using a variable called ϕ_r to control the current set point, as shown in Eq. (9).

Implementation of the Numerical Model on Code Saturne

The software Code_Saturne v. 2.0 electric arc module was used for the 3D transient model of the 3-Phase plasma torch [27]. This CFD software is based on the SIMPLEC algorithm and a fully implicit resolution. A 5 μ s time-step was used and the study is partitioned among eight processors (Intel Xeon 2.66 GHz). One single iteration requires almost 1 min and 30 s. The simulation initialisation (5 ms simulated), takes about 1,000 iterations, i.e. 1 day and 9 h of calculation. Indeed, to ignite the first arcs at the first time-steps, a hot zone at 6,000 K is artificially implemented between the three electrodes and the current target is set during 5 ms from 5 to 400 A.

Because of converging model issues and to simplify current waveform, we do not impose current density on the electrodes but current flowing in the arc. This current is obtained by integrating the current density on three planes located between the three electrodes. At each time-step (n), the ϕ_r coefficient is fitted to maintain the sum of the three absolute measured currents to the set point current (400 A) from the following expression (9):

$$\phi_r^n = \frac{I_{\text{target}}}{I_{\text{measured}}} \phi_r^{n-1} \quad (9)$$

By contrast with 3-Phase AC arc furnaces used in metallurgy where the arcs transit via molten metal as star neutral point, the system studied herein has no ground connected neutral point and is assimilated to a triangular configuration as shown by Ravary et al. [12] and Weidong et al. [13]. Generally, only one arc can exist at one time and two arcs can only coexist during a brief period of time. We suppose that each new arc disturbs the previous one via a magnetic effect, or the joule effect becomes insufficient to maintain two arcs at the same time. Arc discharge then follows the maximal electric gap potential, and each electrode plays alternatively the role of mass, cathode, mass and anode. One period is decomposed into the generation by rotation of 6 arcs, with an arc life duration about one-sixth of the period. Assuming a small oscillation at the electrical gap, we impose a constant value for the sum of the currents measured on the three planes between the electrodes [17]. In the case of a phase delay or a lacking arc, this method gives a greater degree of freedom to the model, and shows results close to the experimental waveforms.

Comparison of MHD Modeling with Experimental Results

The comparison of the results obtained with the high-speed camera and with the MHD model is shown in Fig. 4. First, the results of the MHD model show that the current density field is not exactly in line with the temperature field for a V-shaped arc. Generally, the arc core radius is defined by the radial distance from the centre of the line to the point where the current density is two orders of magnitude smaller than the maximum current density, as assumed by Selvan et al. [27] and Lebouvier et al. [28]. In this study, to correlate the

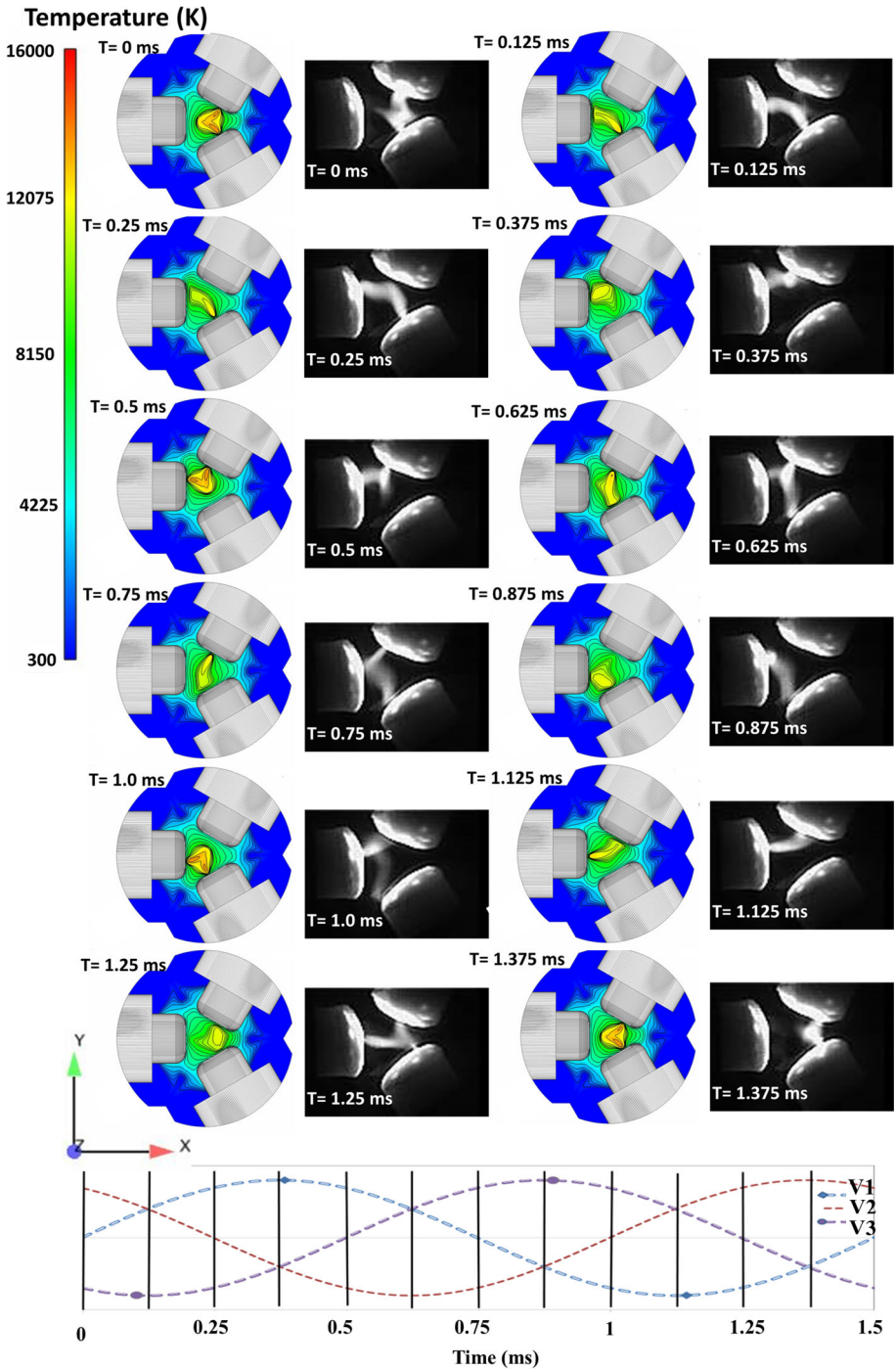


Fig. 4 Comparison of the temperature fields in a cross-section located in a plan containing the 3 electrode axes (*left*) with the arc video sequence (*right*). Images are time-correlated with theoretical line voltages; the 12 vertical lines in the voltage waveforms indicate the time for each image acquisition

image sequence to the results of the MHD model, we assume that the arc can be superposed on the temperature field. In the middle of the arc column, the high temperature zone is partially outside of the main current density zone when the arc is V-shaped. This point was already demonstrated by Hui et al. [29].

Figure 4 shows a cross projection view under the electrode axes of the decomposition of the arc motion with a 0.125 ms time step during almost one period (1.35 ms). At the bottom of the figure is shown the evolution of the phase voltage corresponding to an ideal 3-Phase AC sinusoidal signal. The images have been time-correlated with the line voltage signals. A $5\text{Nm}^3\text{h}^{-1}$ nitrogen flow rate was used in both cases. Numerical results were obtained for a 400 A imposed peak current, which gives a 150–200 A RMS current and a sinusoidal voltage waveform. In the experimental setup, a 150–200 A RMS current is used and the voltage waveform is non-sinusoidal (3-Phase chopper-inverter output or square modified waveform). However, it has been demonstrated that the voltage waveform shape has a negligible influence on the current waveform as discussed in detail further on in the paper.

The sequence displayed in Fig. 4 shows the six chronological arc formations in each period and that the arc behaviors observed experimentally and numerically are almost identical. There is a good correlation between the arc behaviors obtained experimentally and numerically. However, the MHD modeling gives a perfectly reproduced arc motion whereas it is more probabilistic in the experimental setup. With the MHD modeling, the arcs are I-shaped only (e.g. at $t = 0.125$ ms) or V-shaped (e.g. at $t = 0$ ms) while experimental arcs can show different geometries which can be classified into four main traditional shapes as already reported in the literature related to different plasma systems: I, V, W, or S, respectively [12, 13, 30–33]. These experimentally-observed W or S arc shapes could be induced by the electrode tip geometry or the arc root position.

These differences could be explained by separating the arc discharge in two cases: arc root position and arc motion. Regarding the arc root position, the MHD model results have shown that heat transmitted by the mass flow emanating from the electrode jets helps initiate new arc roots. On the $t = 0$ ms image of the simulation, the arc is characterized by two vapour jets. The two jets clash halfway between the two-electrode tip gap, and the enthalpy emanating from the two electrode vapour jets is directed towards the centre of the inactive electrode. In the experimental image, the clash is not stable as shown at $t = 0, 0.375, 0.5, 1.0$ ms, and the enthalpy is not transmitted to the centre of the inactive electrode. So we suppose that the electrode roughness and shape modify the arc root position and the arc shape.

Regarding the arc shape, the arc column's motion is induced by the combination of magnetic and hydrodynamic forces. For example, in the simulation at $t = 0.125$ to 0.25 ms, the arc moves towards the third electrode. The model shows that decreasing the frequency to 50 Hz increases the maximum arc elongation. When the gradient of the electrical potential becomes sufficient between the inactive electrode and the arc column, a new arc root ignites and an arc root switches off, as shown at $t = 0.375$ ms. The magnetic pressure of the new arc root increases and pushes the arc column and the arc root towards the next inactive electrode ($t = 0.5$ ms). This periodic mechanism is reproduced three times per period. Because the arc root position slightly differs in the experimental set-up, the arc shape is also slightly different.

Furthermore, in the experiment, the discharge sometimes appears unbalanced. In this case, the electrode jets are not directed towards the inter-electrode zone but toward the electrode periphery, as shown in ref [16]. The temperature between two electrodes decreases and the electrical conductivity becomes insufficient to ignite a new arc in the

zone. This point underlines the key feature of the heat transmitted by the electrode jet within the inter-electrode gap for the arc ignition.

However from the video sequence, we can also observe that the arc root preferentially occurs on a hot electrode zone which gives a certain recurrence on the position of the arc root birth. This shows that the electrode temperature could also have a significant influence on arc ignition.

To summarize, the position of the new arc root and the arc motion modify the arc shape. We suppose that electrode roughness and geometry also electrode hot spot modify the arc behavior. As mentioned in a previous paper [17], the heat transmitted by the electrode jet and the arc modifies the discharge stability. This is the reason why the experimental results obtained with the high-speed camera sometimes differ from the MHD modeling.

To assess the model validity, comparisons of the numerical results and arc motion obtained with the high-speed camera for different cases were considered.

Influence of the Current

The MHD model results for a current lower than 100 A RMS have highlighted a particular arc discharge shape. The arc position follows a Y shape, which is similar to the arc behavior observed with the high-speed camera when the system is set below 100 A RMS. This behavior has been observed but not recorded due to the system instability under these conditions [17]. The discharge with a Y shape shows that the electrode jets or Lorentz forces are not enough to influence the arc motion with a current lower than 100 A RMS. The model shows that the imposed current changes the electrode jet velocity as well as the arc motion. In addition, the results of the MHD modeling show that the arcs are located downstream of the electrode axes, which can hardly be observed experimentally. It is worth pointing out that the same arc behavior was observed when increasing the frequency (2,000 Hz) in the MHD model. This shows that frequency is a key parameter in the influence of the Lorentz forces on the arc motion.

By increasing the current to 300 A RMS, the arc V shape is amplified and reproduced by the MHD model as shown in Fig. 5. This indicates that the Lorentz forces and the electrode jet velocity are well simulated by the model. By comparing the arc velocity obtained with the model and experiment at 300 A RMS, the arc root velocity is almost similar. It was estimated at around 50 m s^{-1} with the high-speed camera, whereas it reaches a maximal velocity of 40 m s^{-1} in the model. Also, in the experimental setup, increasing the current raises the electrode hotspot size and the arc and electrode jet velocities.

Influence of the Inter-Electrode Gap

By increasing the inter-electrode gap from 5.5 to 13 mm, the MHD model reproduces the trend of the experimental arc behavior, as demonstrated in Fig. 6. The electrode jets interaction is unbalanced which produces more deflected arcs in both cases. However, as opposed to the modelling, the arc root is often located at the bottom of the electrode tips or on a hot spot position in the experimental set up. The repulsive magnetic forces on the most deflected arc column increase the arc motion within the inter-electrode gap. Elsewhere, in the experimental setup, the increase of the inter-electrode gap tends to stabilize the electrical 3-Phase arc discharge.

To conclude this parametric comparison, the MHD model globally reproduced an arc behavior similar to the one observed with the high-speed camera for different cases. Below 100 A, the model shows the Y shape of the 3-Phase discharge. At 150–200 A, arc behavior

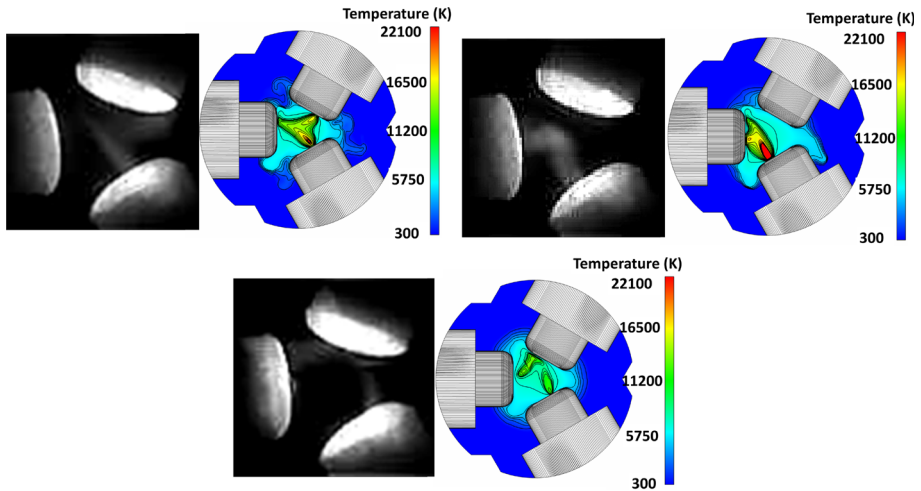


Fig. 5 Comparison between extracted arc images and temperature fields, in a cross-section located in a plan containing the three electrode axes at 300 A RMS

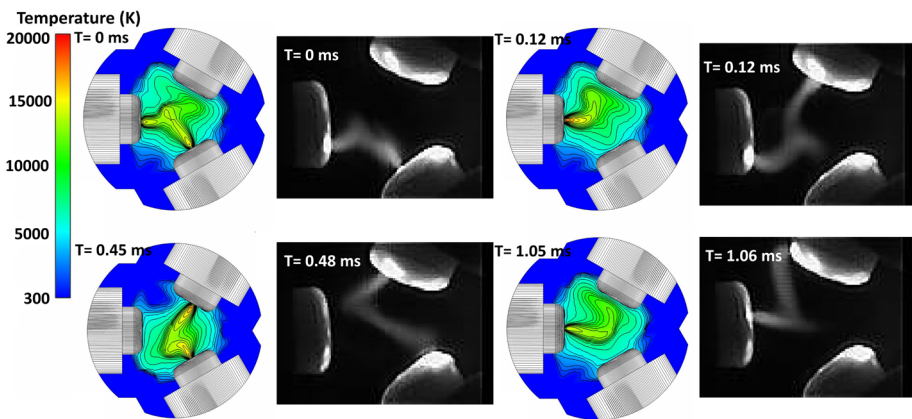


Fig. 6 Comparison of the temperature fields at 150 A RMS for an 13.5 mm electrode gap length (*left*) with the arc video sequence for a 13 mm electrode gap (*right*)

for a stabilized system is simulated, and the amplified V shape of the arc is highlighted by increasing the current. Regarding the inter-electrode gap, similar trends of arc behavior can be derived from experimental and numerical results. A final test has been carried out by increasing the plasma gas flow rate. Results show very little influence of this flow rate. These results confirm the strong influence of the electrode jets and Lorentz forces on arc motion. They also confirm the influence of the heat transmitted by the electrode jet within the inter-electrode gap to ignite new arc roots. These forces are reproduced by the MHD modeling as shown in Fig. 7. Globally, some slight differences have been observed regarding arc root positions and arc shape. To validate this model, the electrical waveforms are compared.

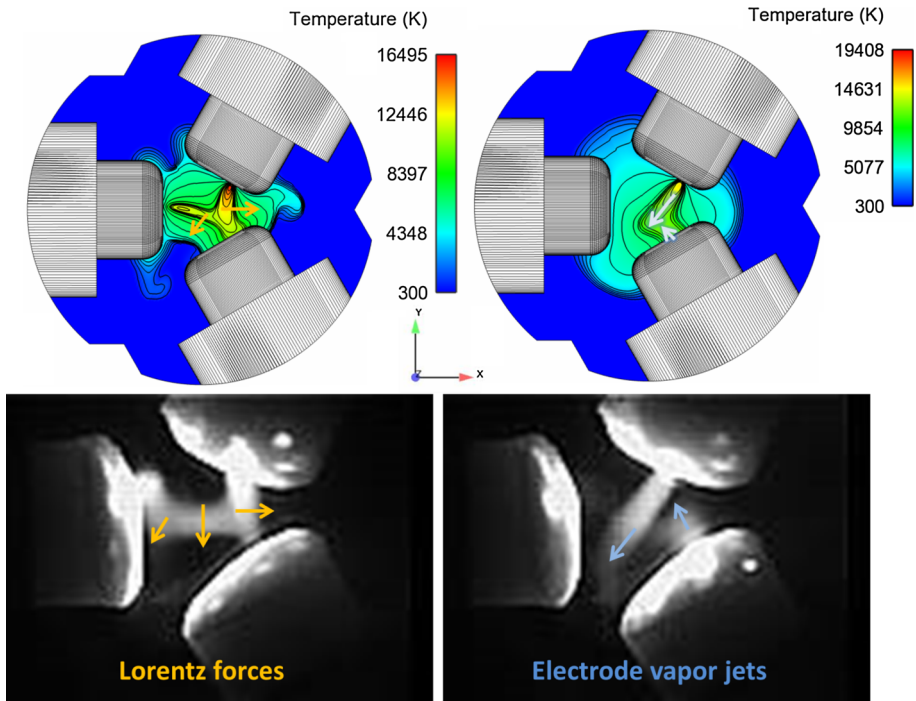


Fig. 7 Schematic representation illustrated on the pictures of the influence of the Lorentz forces (*left*) and the electrode jets (*right*) on the arc motion (*left*) and by the electrodes jet (*right*)

Comparison of Electrical Waveforms

As previously mentioned, the 3-Phase system is assimilated to a triangle configuration with no ground-connected neutral point and, generally, only one arc exists at one time. Assuming a symmetrical and purely resistive system, the arc discharge follows the maximal potential difference. In the MHD modeling, the voltage shape is imposed with sinusoidal waveform whereas the actual voltage in the experimental setup (thyristor technology) has a modified square waveform which significantly differs from a sinusoidal signal. The current waveform obtained for a sinusoidal line voltage waveform and a 3-Phase chopper-inverter output voltage waveform (modified square) have been compared in Fig. 8. Assuming slight amplitudes of the voltage waveforms, both current waveforms are similar. The line current waveform remains close to zero during one arc lifetime between alternating negative and positive peaks, and follows the line voltage. Experimental and numerical current waveforms could then be compared with a slight influence of the actual voltage waveform.

The voltage and current waveforms for one phase (i. e. phase Number 3) obtained with the MHD modeling were compared with the experimental oscillograms measured on the same phase, as shown in Fig. 9. The experimental current signal is not much different from the modified square waveform given on the top of Fig. 8. As observed, the experimental current oscillograms present some slight differences with the numerical waveforms. Peak values are around 300 A for the numerical waveform and about 200 A in the oscillograms. Focusing on the MHD current waveform during one alternation, one arc delivers a higher

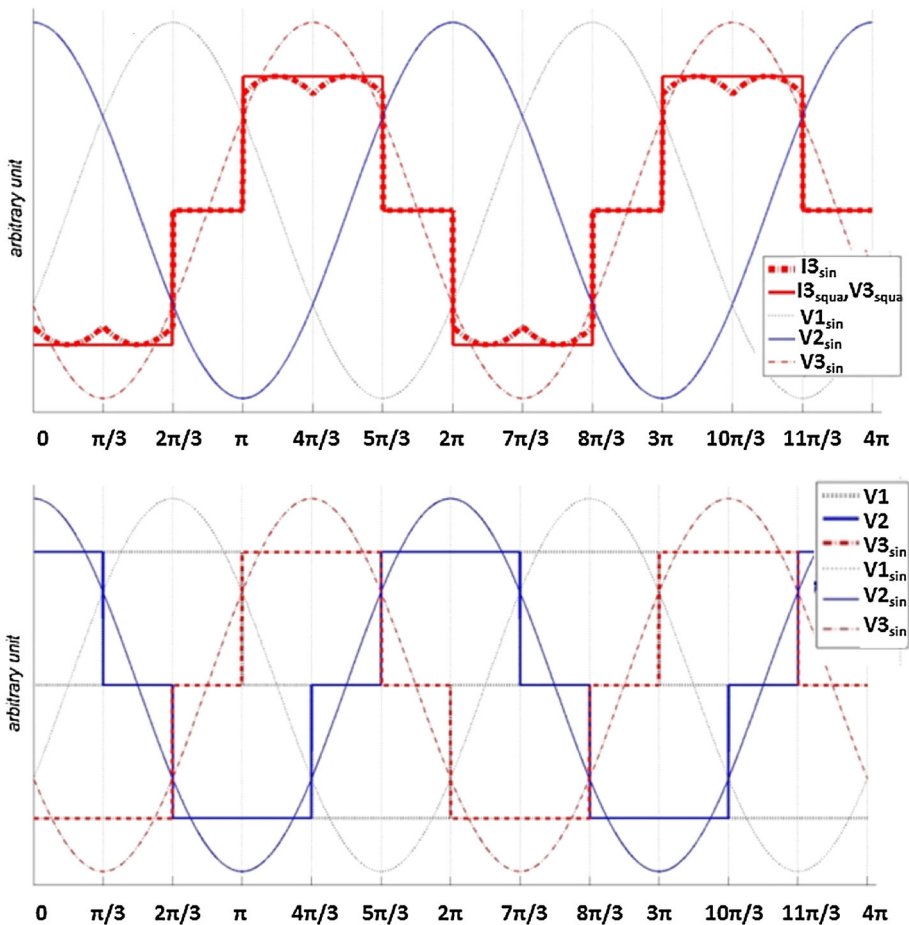


Fig. 8 On the top, comparison of theoretical current waveforms obtained with a square and a sinusoidal voltage waveforms (the thick line is the Number 3 phase current, and the thin lines the phase voltages). At the bottom, comparison between sinusoidal and 3-Phase chopper-inverter output voltage waveforms

current than the experimental oscillogram. As demonstrated in a previous paper [21], the peak current increases with a V-shaped arc whereas it decreases with an I-shaped arc/. As part of the current flows between the two other electrodes and through two planes to control the current, the instantaneous current differs. The current does not stay at zero during one arc lifetime, but it shows a quick negative-to-positive alternation. This specific current waveform is also sometimes experimentally observed. Also the experimental voltage oscillogram has a square waveform with a sharp negative-to-positive alternation and does not stay at zero. To summarize, some differences are observed between experimental and numerical electrical waveforms, and particularly in the current-to-voltage phase difference.

In Table 3, we can observe that the experimental RMS voltage is more or less stable at a value of 35 V, regardless of the operating parameters, except at 50 A (case c), where the RMS voltage increases slightly to 42 V. RMS voltage is between 25 and 30 % of the experimental one with an average value around 10 V as a result of the non-inclusion of the

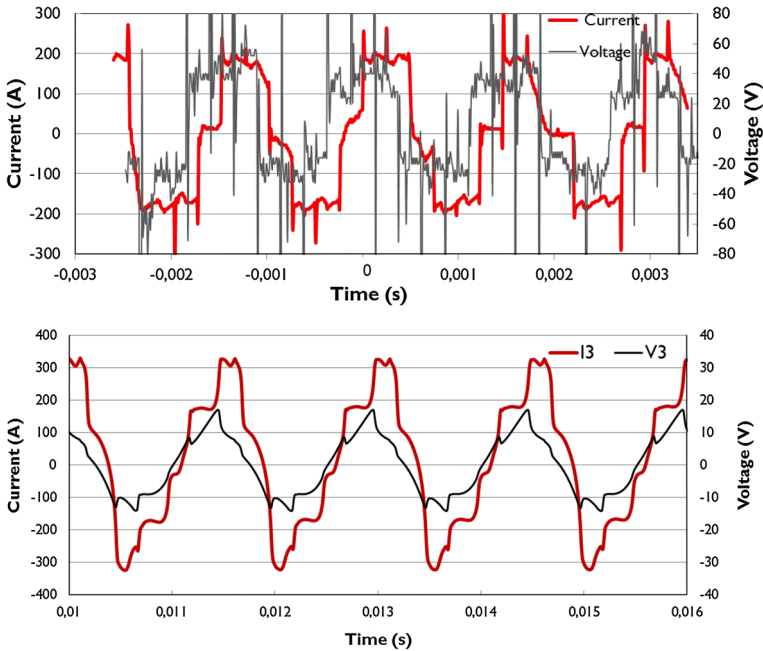


Fig. 9 Comparison of the experimental voltage and current waveforms for a 150–200 A RMS (*top*) and obtained with the MHD modeling for a 400 A peak current. The numerical current is represented by the *thick line* and the experimental voltage by the *thin line*

Table 3 Averaged current and voltage for the different cases

		Case a	Case b	Case c	Case d	Case e
RMS current value (A)	Exp	150–200	50–100	300	150–200	150–200
	Num	200	100	300	200	200
Inter-electrode gap (mm)		5.5	5.5	5.5	5.5	5.5
Gas flow rate (Nm ³ h ⁻¹)		5	5	5	5	7
Mean voltage value (V)	Exp ^a	35	42	35	37	36
	Num	10	11	9.6	16	9.7
Power (kW)	Exp	11–16	3–9	22–30	11–16	11–16
	Num	4.9	3.0	5.7	7.75	4.7

^a Experimental voltage deviation is around 1.8 V except for case b where it is around 3.5 V [16]

near-electrodes sheath voltage drop which generally varies between 3 and 10 V for high-current arcs [34]. However, as previously mentioned some other differences are observed between experimental and numerical electrical waveforms, and particularly in the current-to-voltage phase shift.

We have observed that the electrode tip erosion progressively induces an angle ranging from 10° to 20° with the electrode axis, as shown in Fig. 10 that could modify the arc behavior. To observe this influence, the grid mesh was modified by considering conical shape due to geometry-meshing issues in the MHD model.

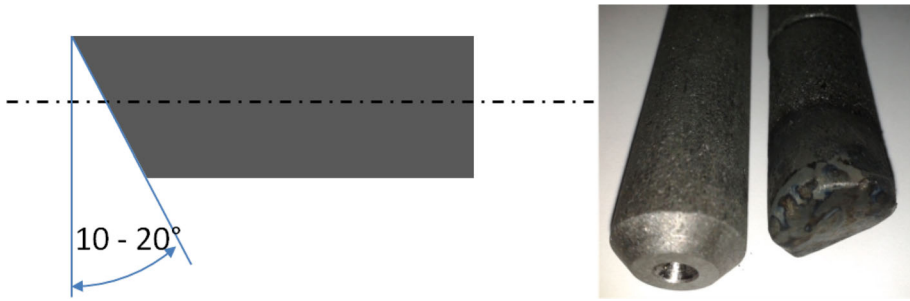


Fig. 10 *Left*, a schematic geometry of the electrodes sublimation with a 10–20° after 3-Phase plasma torch. *Right*, electrodes geometry before and after operation

Influence of the Electrode Tip Geometry of the MHD Modeling

The grid mesh was modified by changing the shape of the electrode tip. However, the influence of electromagnetic forces generated by the curvature of the charge carriers within the electrodes can have an influence on the motion of the arc roots. To improve arc/electrode thermal transfer and the simulation of the arc root and hotspot positions, a model of thermal transfer with the electrodes was implemented. The graphite electrodes are incorporated into the computational domain (zone DD'D''E''E'E). The methodology used to integrate the solid phase in a model of fluid mechanics was entirely based on the work of [35, 36]. This step is not trivial, as it involves removing the diffusivity from the material/fluid faces. Gradient reconstruction in the solid/fluid interface is removed and the continuity of thermophysical properties is calculated by harmonic interpolations. The graphite properties were taken from different databases. For the specific heat capacity, we took the following Eq. (10) given by the NIST database [37]:

$$C_p = -1,43668.10^9 T^{-4} + 1,59309.10^7 T^{-3} - 4,34493.10^4 T^{-2} - 9,03725.10^1 T^{-1} + 9,11129.10^{-6} T + 2253,74 \tag{10}$$

For thermal conductivity, we used the following relationship: $\lambda = 470 - T/10$ if $\lambda > 100$ if $\lambda = 100$ [38]

For electrical conductivity, we considered a constant value of $1.10^5 \Omega \text{ m}^{-1}$ as well as a $1,700 \text{ kg m}^{-3}$ density [38].

The grid mesh is based on the previous one (Fig. 11). A non-uniform hexahedral mesh is used in the electrode and in all the areas of the computational fluid domain. To observe the electrode tip geometry influence, the grid mesh was modified by considering the conical shape caused by geometry-meshing issues, and the angle was overestimated. The mesh contains approximately 900,000 nodes. The boundary conditions were not modified, except that the electrical potential waveforms are now imposed on the DE surfaces.

Current is now controlled within the electrodes by the integral of the current density on the three planes D'E' perpendicular to the electrode axes. We impose a current value for the sum of the three calculated currents. Only one arc exists at a time. Then the imposed current value is twice that of the required current as the arc current is calculated two times.

The MHD modeling was successfully implemented and it automatically simulates arc ignition, extinction, and motion between the three electrode tips. Results exhibited in Fig. 12 show that the arc behavior differs from the previous model. The arc shapes differ from previous results and clearly approach the arc behavior observed with the high-speed

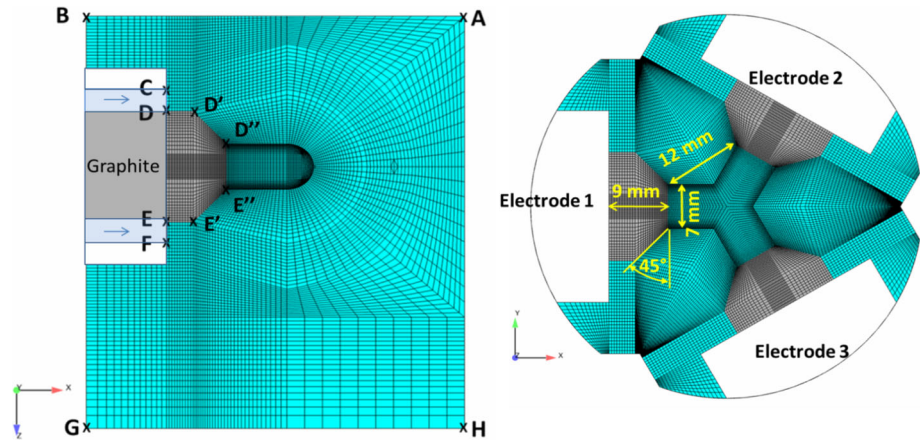


Fig. 11 Computational grid of the 3-Phase plasma torch and cross-section of the computational grid on the three electrodes gap

camera (I, V, U, W, S). With this model, the arc root position remains fairly constant. The memory effect of the middle plays a major role in this simulation. The previous arc position will then be crucial to the discharge behavior. Each arc provided in this hot column induces a slight motion on the arc discharge channel. This motion is influenced by the electrode jets and Lorentz forces. The enthalpy transmitted by the electrodes jets can sometimes modify the arc root position ($t = 4.2 - 4.3$ ms). These arc roots are initiated when the jet-transmitted enthalpy is close to the electrode area.

With this model, changing the electrode geometry tip induces an axial motion on the arc directed towards the outlet of the system. This axial motion of the arcs is displayed with front views in Fig. 13. It explains the W or S arc shapes obtained experimentally. In the first existing time of an arc, the arc column motion is not influenced by the electrodes jets and is directed towards the outlet of the computational domain. With the jets expansion, the arcs appear as a W shape. Regarding the S shape, the normal directions of the electrode tip of the two arc roots do not converge which produces these particular arc shapes ($t = 5.0$ ms Fig. 12).

In the arc behavior previously discussed, the heat transmitted by the electrode vapour jet directed towards the inter-electrode zone contributes to the ignition of a new arc root. With the conical electrode shape, the electrode jets are not directed towards the inter-electrode gap center, as shown in Fig. 12. This arc position prevents the transfer of enthalpy towards the inactive electrode and disturbs the ignition of the new arc at the potential maximal electrical difference. With the rotation of the electrical potential field within the inter-electrode gap, the arc switches off when the electrical potential difference nears zero, then the next arc ignites. This produces an arc ignition delay, as shown in Fig. 14. As displayed in Fig. 15, the electrical waveforms are close to the experimental oscillograms. Also the phase shift between current and voltage (under $\pi/6$ in the previous MHD model's results) is around $\pi/3$ here, which is close to the experimental results. The phase shift observed in experimental oscillograms generally varies between $\pi/6$ and $\pi/3$, corresponding to a power factor between 0.866 and 0.5 respectively. Therefore, this power factor is not negligible in this 3-Phase system. However, at such operating frequency (660–680 Hz), the inductive effects are negligible. We can then assume that the arcs ignition is not in phase with the

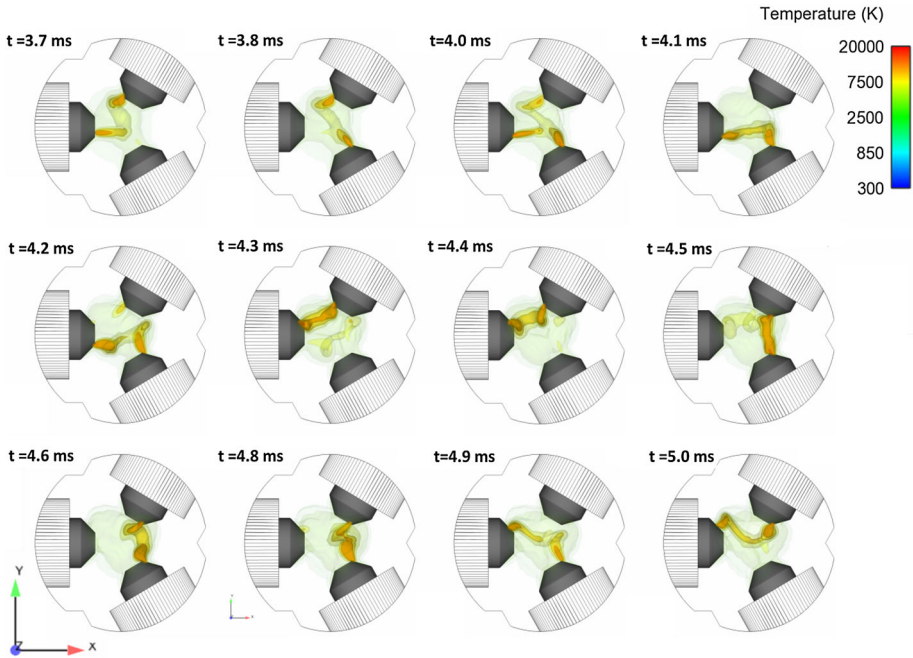


Fig. 12 Arcs behavior between the 3 electrodes, by integrating the electrode into the computational domain and by modifying the electrode tip shape. The arc and hot zone are represented by 15,000; 10,000; 7,500; 5,000; and 2,500 K isosurface temperatures. Electrodes are colored in *black*

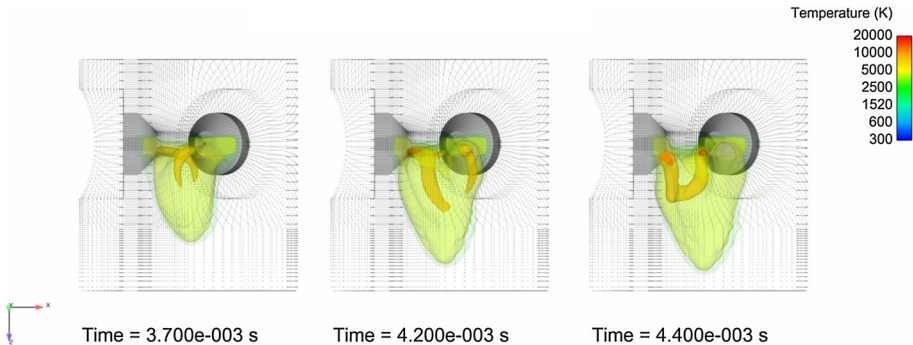


Fig. 13 Arcs behavior between the 3 electrodes displayed with a front view

voltage in the experimental setup. First, small differences in the arc root position, on the arc extinction, or the existence of an intensive hot spot modify or disturb the system, and the arc can ignite at the periphery of the inter-electrode gap as observed with the high-speed camera [17]. Next, the arcs move towards the outlet of the torch, which cannot be observed with the camera. With the arc elongation and the delay in arc ignition, the voltage increases.

In the experimental oscillograms, the RMS phase voltage is around 35 V. With this model, the numerical RMS phase voltage is around 30–40 V with a maximum peak value

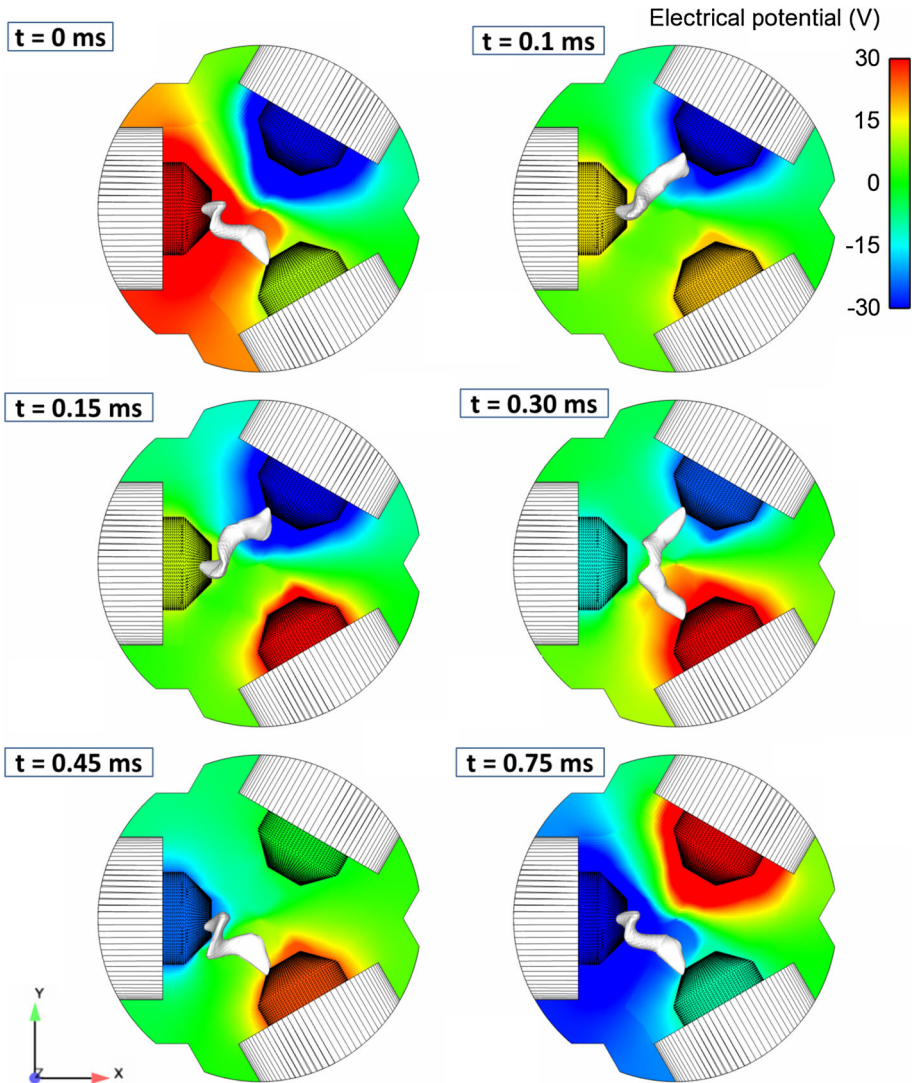


Fig. 14 Arc behavior represented by a 12,000 K isosurface (*white*) in the inter-electrode gap with conical electrodes. The electrical potential field (value represented in the *color map*) is displayed in a cross-section under the center of the electrodes

of 70 V (Fig. 15) which explains the differences of the previous model with the experimental voltage. Furthermore, by imposing current on the electrodes, the current waveform is close to the one obtained experimentally. However, these values do not take into account the phase shift contrary to the power. The dissipated power is between 10 and 15 kW with the model and between 12 and 20 kW in the experimental set-up. These results suggest that this model is the most representative of the actual arcs behavior. Therefore, arcs have an axial motion which could not be observed with the high-speed camera.

This simulation reproduces the unbalanced arc discharge behavior observed with the high-speed camera (Fig. 16). In this case the arcs between two electrodes are skipped. This

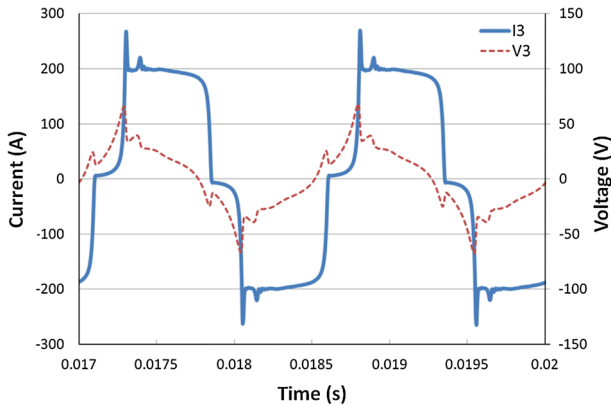


Fig. 15 Current and voltage waveforms obtained with conical electrode tips for a 150 A RMS phase current. The current is represented by a *thick line* and the voltage by a *thin line*

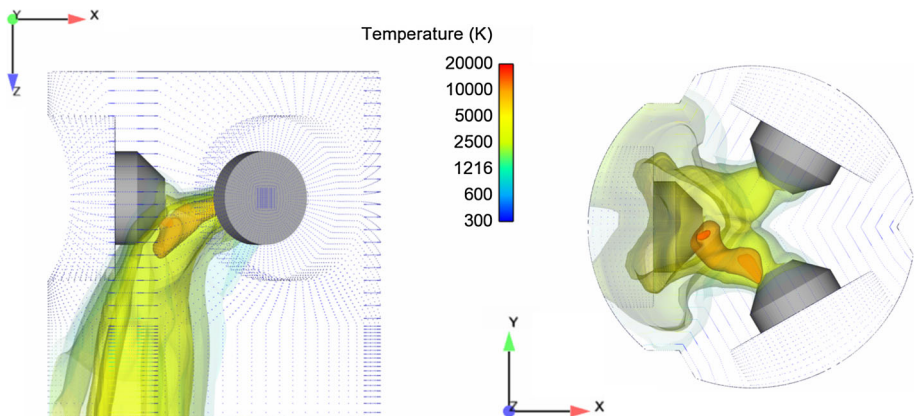


Fig. 16 Thermal flux generated by the 3-Phase discharge displayed with a front view when the discharge is unbalanced

unbalanced 3-Phase discharge drastically alters the temperature field profiles of the plasma flow. As shown in Fig. 16, a large majority of the heat flux is directed towards the walls. The discharge stability is therefore a key feature on the 3-Phase plasma torch system. In a previous paper, the influence of the parameters on the stability of the 3-Phase discharge has been investigated [21].

A further test was conducted by doubling the diameter of the computational domain ($\varnothing = 120$ mm). The minimal distance between two electrodes is 61.5 mm (Fig. 17). The results show that the interaction of the electrode jets does not have more influence on the behavior of the arc discharge. This discharge is therefore balanced with a typical ‘Y’ arc discharge shape. This shape was previously obtained with the previous model and cylindrical electrodes by decreasing the current or by increasing the frequency. This configuration seems to be the solution to stabilize the discharge. However, to initiate the discharge, the electrodes must be in contact. By diverting the electrodes, the discharge will most

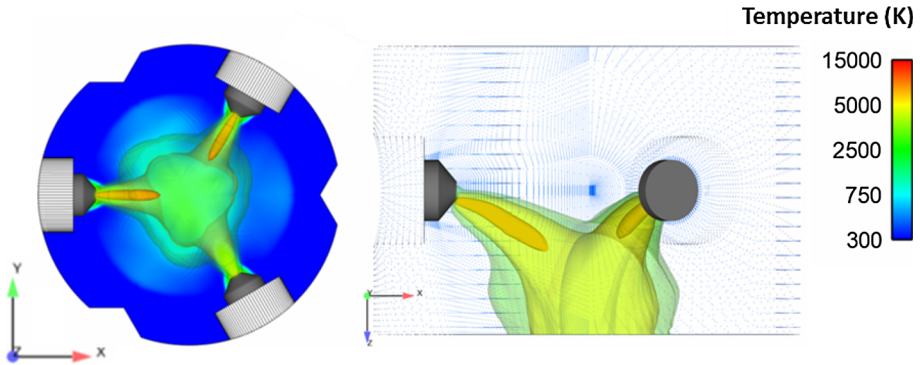


Fig. 17 Arcs and thermal flux obtained by doubling the diameter of the arc zone ($\varnothing = 120$ mm) with a bottom view (*left*) and a front view (*right*)

likely be unbalanced before reaching the desired configuration. One solution would be to install another plasma system upstream as intended by the device [39] or to increase the frequency. It should be noted that the increase of the inter-electrode gap does not significantly change the dissipated power in the system (around 20 kW) but the phase difference between the voltage and current decreases.

Conclusion

A MHD model of the 3-Phase plasma torch was recently developed. This model automatically simulates the arcs ignition, extinction, and produces a particular arc motion between the three electrode tips. The arc motion was analysed using a high-speed video camera, and the comparison between experimental and numerical results is presented in this paper. This comparison shows that the arc behavior is consistent with the results obtained with our model for 100–300 A RMS currents and various inter-electrode gaps.

Regarding the electrical signals, voltage, current–voltage phase delay and power were not accurately reproduced with the previous MHD model. This study shows that the electrode tip geometry has an important influence on the arc behavior and electrical waveforms. By modifying the model with the conically-shaped electrode tip, the numerical results correspond better to what is observed. In particular, the current–voltage phase shift is fairly reproduced showing that this phase shift is probably due to the arc ignition delay. The arcs' axial motion is directed towards the outlet which could not be observed with the high-speed camera. The previous model shown that the enthalpy transmitted by the electrode jets on the inactive electrode helps with arc ignition. The transfer of enthalpy towards the inactive electrode is prevented with the axial motion of the arc or when the arc roots are in the periphery of the inter-electrode gap. This produces a phase delay which increases the electrical potential, and the increase of the arc length raises the dissipated power close to the experimental results.

To conclude, results show a fair correlation between MHD modeling and arcs' video, both regarding the global arc behavior and the current and voltage waveforms. Subsequently, the developed MHD model is a powerful tool to investigate the experimental arc behavior based on the operating conditions. This study is likely to pave the way for a better understanding of 3-Phase discharges, whose technologies are interesting for many application fields.

Acknowledgments The authors gratefully acknowledge the “Provence–Alpes–Côte d’Azur–PACA” French administrative region for its financial support and M. Sabri Takali for his technical support.

References

- Gleizes A, Gonzalez JJ, Freton P (2005) Thermal plasma modeling. *J Phys D Appl Phys* 38(9):153–183
- Trelles JP, Chazelas C, Vardelle A, Heberlein JV (2009) Arc plasma torch modeling. *J Therm Spray Technol* 18(5):728–752
- Fauchais P, Montavon G, Bertrand G (2010) From powders to thermally sprayed coatings. *J Therm Spray Technol* 19(1):56–80
- Fabry F, Rehmet C, Rohani V and Fulcheri L (2013) Waste gasification by thermal plasma: a review. *Waste Biomass Valor* 3(4). doi:10.1007/s12649-013-9201-7
- Heberlein J, Murphy AB (2008) Thermal plasma waste treatment. *J Phys D Appl Phys* 41:053001
- Matveev IB, Rosocha LA (2010) Guest editorial classification of plasma systems for plasma-assisted combustion. *IEEE Trans Plasma Sci* 38(12):3257–3264
- Liu Y, Tanaka M, Choi S and Watanabe T (2013) Investigation of spatial characteristics of multi-phase AC arc combined with in situ particle measurement. In: 21st International symposium on plasma chemistry (ISPC 21) August 2013 Cairns Australia
- Popov SD, Rutberg AF, Safronov AA (2007) The use of AC plasma generators for operation as a part of plasma reactor: special features. *High Temp* 45(1):1–6
- Rutberg PhG, Safronov AA, Popov SD, Surov AV, Nakonechny GhV (2005) Multiphase stationary plasma generators working on oxidizing media. *Plasma Phys Control Fusion* 47:1681
- Gorbunov VP, Kushev SA, Lukyanov SA, GhV Nakonechny, Popov SD, Popov VE, Spodobin VA, Serba EO (2007) Characteristic features of operation of high-voltage electric arc plasma generators with rod electrodes and power from 5 up to 50 kW in a pilot plasma chemical unit. 16th IEEE Int Pulsed Power Conf 2:1560–1564
- Rutberg PG, Lukyanov SA, Kiselev AA, Kushev SA, Nakonechny GV, Nikonov AV, Surov AV (2011) Investigation of parameters of the three phase high-voltage alternating current plasma generator with power up to 100 kW working on steam. *J Phys Conf Series* 275(1):012006
- Ravary B, Fulcheri L, Bakken JA, Flamant G, Fabry F (1999) Influence of the electromagnetic forces on momentum and heat transfer in a 3-phase AC plasma reactor. *Plasma Chem Plasma Process* 19(1):69–89
- Weidong X, Fulcheri L, Gonzalez-Aguilar J, Hui L, Gruenberger T (2006) Characterization of a 3-phase AC free burning arc plasma. *Plasma Sci Technol* 8:156–163
- Colombo V, Concetti A, Ghedini E, Dallavalle S, Vancini M (2009) High-speed imaging in plasma arc cutting: a review and new developments. *Plasma Sources Sci Technol* 18:023001
- Colombo V, Concetti A, Ghedini E, Nemchinsky V (2010) High-speed imaging investigation of transition phenomena in the pilot arc phase in Hf cathodes for plasma arc cutting. *Plasma Sources Sci Technol* 19:065025
- Colombo V, Concetti A, Ghedini E, Rotundo F, Sanibondi P, Boselli M, Dallavalle S, Gherardi M, Nemchinsky V, Vancini M (2012) Advances in plasma arc cutting technology: the experimental part of an integrated approach. *Plasma Chem Plasma Process* 32(3):411–426
- Rehmet C, Fabry F, Rohani V, Cauneau F, Fulcheri L (2013) High speed video camera and electrical signal analyses of arcs behavior in a 3-Phase AC arc plasma torch. *Plasma Chem Plasma Process* 33:779–796. doi:10.1007/s11090-013-9458-4
- Larsen H (1996) AC electric arc models for a laboratory set-up and a silicon metal furnace. NTH, University of Trondheim, Department of metallurgy, Norway
- Bakken J, Gu L, Larsen H, Sevastyanenko V (1997) Numerical modeling of electric arcs. *J Eng Phys Thermophys* 70(4):530–543
- Saersdottir G, Bakken J, Sevastyanenko V, Gu L (2001) High-power AC arcs in metallurgical furnaces. *High Temp Mater Process* 5:21–43
- Rehmet C, Rohani V, Cauneau F, Fulcheri L (2013) 3D unsteady state MHD modeling of a 3-Phase AC hot graphite electrodes plasma torch. *Plasma Chem Plasma Process* 33(2):491–515
- Archambeau F, Mechitoua N, Sakiz M (2004) Code Saturne: a finite volume code for the computation of turbulent incompressible flows industrial applications. *Int J Finite* 1:1–62
- <http://www.olympus-ims.com/en/hsv-products/i-speed-fs/>
- Pateyron B “T&TWinner” free download from <http://www.unilim.fr/spts> or <http://ttwinner.free.fr>
- Naghizadeh-Kashani Y, Cressault Y, Gleizes A (2002) Net emission coefficient of air thermal plasmas. *J Phys D Appl Phys* 35:2925–2934
- Salome, <http://www.salome-platform.org/>

27. Selvan B, Ramachandran K, Sreekumar KP, Thiyagarajan TK, Ananthapadmanabhan PV (2009) Numerical and experimental studies on DC plasma spray torch. *Vacuum* 84(4):444–452
28. Lebouvier A, Delalondre C, Fresnet F, Boch V, Rohani V, Cauneau F, Fulcheri L (2011) Three-dimensional unsteady MHD modeling of a low-current high-voltage nontransferred DC plasma torch operating with air. *IEEE Trans Plasma Sci* 39:1889–1899
29. Hui Y, Yan WZ, Wu CK (2000) Numerical investigation of flow field of a dual-jet plasma generator. *Plasma Sci Technol* 2:141
30. Barthelemy B (2003) Combustion-vitrification de déchets radioactifs par plasma d'arc: Modélisation de la thermique et de la dynamique; Thèse de l'Université de Limoges, soutenue le 12 juin 2003 (in French)
31. Schnick M, Wilhelm G, Lohse M, Füssel U, Murphy AB (2011) Three-dimensional modelling of arc behaviour and gas shield quality in tandem gas-metal arc welding using anti-phase pulse synchronization. *J Phys D Appl Phys* 44:185205
32. Colombo V, Ghedini E, Boselli M, Sanibondi P, Concetti A (2011) 3D static and time-dependent modelling of a dc transferred arc twin torch system. *J Phys D Appl Phys* 44:194005
33. Tang KM, Yan JD, Chapman C, Fang MTC (2010) Three-dimensional modelling of a DC arc plasma in a twin-torch system. *J Phys D Appl Phys* 43:345201
34. Lebouvier A, Delalondre C, Fresnet F, Cauneau F, Fulcheri L (2012) 3D MHD modelling of low current-high voltage DC plasma torch under restrike mode. *J Phys D Appl Phys* 45:025204
35. Chemartin L, Lalande P, Delalondre C, Cheron B, Lago F (2009) Modelling and simulation of unsteady dc electric arcs and their interactions with electrodes. *J Phys D Appl Phys* 44:194003
36. Borel D (2013) Étude numérique et expérimentale des transferts thermiques dans un plasma d'arc Application au soudage à l'arc TIG, 2013. Thèse Doctorale de l'université de Rouen (in French)
37. NIST Database, <http://webbook.nist.gov/cgi/cbook.cgi?ID=C7782425&Mask=2>
38. Coulon M, Reyvaan C, Maire J (1994). Le carbone en électrotechnique. *Technique de l'ingénieur, Référence D2660* (in French)
39. Bonet C, Lamos JF, Foex M (1970) Ecoulement permanent de plasma de grande puissance. *Entropie* 34:36–48